ISSN 0389-4010
UDC 621.438
532.5

TECHNICAL REPORT OF NATIONAL AEROSPACE LABORATORY

TR-984T

Three-Dimensional Flows and Loss Generation Mechanisms in a Linear Turbine Rotor Cascade at Various Incidence Conditions

Atsumasa YAMAMOTO, Hiroyuki NOUSE

June 1988

NATIONAL AEROSPACE LABORATORY

CHŌFU, TOKYO, JAPAN

Three-Diemensional Flows and Loss Generation Mechanisms In a Linear Turbine Rotor Cascade at Various Incidence Conditions*

Atsumasa YAMAMOTO**, Hiroyuki NOUSE**

ABSTRACT

The paper describes effects of the incidence on cascade three-dimensional flows and on the associated loss mechanism occurring in a low-speed linear turbine rotor cascade. For five different incidences from 7.2 to -53.3 degrees, the cascade flow was surveyed in detail at fifteen or sixteen planes located axially throughout the cascade. Blade-to-blade flows at the cascade midspan and near the endwalls, meridional flows along the blade surfaces, and static and total pressures within the cascade were analized and the results were represented in three-dimensional forms using vectors, scalar contours and streaklines, from which one could easily understand the extraordinarily complicated cascade flows and the loss generation mechanisms. The present study gives not only new insight into the incidence effects but also adds many solid experimental facts in a quantitative manner to our knowledge of turbine cascade flows.

概　　要

本論文は低速直線タービン動翼列内で生ずる三次元流とそれに伴う損失に及ぼすインシデンスの影響について述べたものである。7.2°から−53.3°の異なる5種類のインシデンスについて，翼列の流れを翼列の軸方向に配置した15又は16個の断面で詳細に測定した。翼スパン中央や翼端面近傍の翼間面 (blade-to-blade) 上の流れ，翼表面に沿う子午面 (meridional) 流れ，翼間での静圧あるいは全圧分布を解析した。その結果は非常に複雑な翼間での流れや損失発生メカニズムを容易に理解できるように，速度ベクトル，スカラー量の等高線，さらに流線を用いて三次元表示した。本研究はインシデンスの影響に関する新しい知見を与えるのみならず，既に知られ又は推定されている知識にも多くの確固とした実験事実を与えるものである。

NOMENCLATURE

C_{ax} = blade axial chord

CP_s = static pressure coefficient based on mass-averaged velocity at Plane 12, $\bar{\bar{V}}_{m,12}$

$= (P_s - \bar{\bar{P}}_{t,0})/(0.5 \times \rho \times \bar{\bar{V}}^2_{m,12})$

CP_t = total pressure loss coefficient based on $\bar{\bar{V}}_{m,12}$

$= (P_{t,0} - P_t)/(0.5 \times \rho \times \bar{\bar{V}}^2_{m,12})$

CV_m = dimensionless resultant velocity normalized by $\bar{\bar{V}}_{m,12}$

H = span of cascade passage

i = incidence

P_s = static pressure

P_t = total pressure

V_m = resultant flow velocity

V_s = magnitude of secondary flow vector normal to the local midspan flow

* Received April 5, 1988

** Aeroengine Division

directions

V_s' = magnitude of secondary flow vector normal to the mass-averaged flow direction

V_z = meridional velocity

W = velocity component projected onto the endwall

Y = spanwise distance from hub endwall

Z = axial distance from blade leading-edge

Δ = interval of contour plot

ρ = density

θ_y = yaw flow angle measured from cascade axial direction

Subscripts

0–12 = number of traverse measuring (S3) planes

g = inlet guide plates

mid = midspan

net = net

z = axial

Superscripts

$\bar{}$ = pitchwise mass-averaged value

$\bar{\bar{}}$ = overall mass-averaged value

INTRODUCTION

The turbine blade row operates at various inlet flow angles (i.e., various incidences), due to the change in rotational speeds of the preceeding blades or of the blades in question. Incidence is one of the most important factors affecting the turbine performance. The overall loss characteristics with incidence variation is well known as shown, for example, by an Ainley's correlation between the cascade overall loss and the incidence (Fig. 67 in [1]) which includes profile loss, secondary loss and annulus (endwall) loss. The profile loss has generally a minimum value at the optimum incidence near zero incidence and increases with incidence change both above and below the optimum. The increase of profile loss above and below the optimum incidence is considered due mainly to the flow separation generated at the blade suction side and the pressure side, respectively. The so-called secondary loss increases with increasing the incidence and this is considered due mainly to passage vortices which are strengthened in the cascade due to increase of flow turning. According to the Ainley's correlation, the annulus endwall loss is very small compared to the other losses and nearly constant regardless of the incidence variation. Much of the above consideration is based on the flow surveys made only upstream and downstream of cascades, but not on detailed flow measurements within cascades. Such loss correlations as described above have been widely used in the turbine design and confirmed valid in many conventional blade rows with relatively sharp leading-edges, but it has not been very clear that such correlations can be valid also for many such advanced blade rows with blunt leading-edges and with high turning as widely adopted in recent air-cooled turbines. In addition, many advanced computational methods recently being developed with high-speed computers have a possibility of predicting losses directly without such empirical correlations. Under these circumstances, more detailed information about the cascade flows and the loss mechanism is urgently needed.

In turbine cascade passages, various kinds of losses exist, such as blade profile loss due to boundary layer development on blade surfaces and flow separation, secondary loss due mainly to passage vortices, endwall loss and tip-leakage loss, corner loss and so on. To study each loss mechanism in cascade three-dimensional flow fields, detailed flow measurements within cascade have been made recently (e.g., [2-12]) but most of them were made only at design or near design incidence. Studies on detailed loss mechanisms (not only on overall loss) aimed to the incidence effects have been very scarce: Langston et al. [3] showed an effect of incidence on the location of a separation saddle point of inlet endwall flows with an ink-trace flow visualiza-

tion technique for two incidences (about zero and +11.8 degrees). Hodson and Dominy [10] have recently reported detailed flow mechanisms under off-design conditions occurring in a high-speed linear cascade of low-pressure turbine blades, based on oil-flow visualization made over the endwall and over the blade surfaces, and based on flow surveys made close to the cascade exit plane. Their oil-flow visualization clearly showed stronger accumulation of low-momentum endwall fluids on the blade suction surface as the incidence increased from −20 to +8.2 degrees. Yamamoto [13] has revealed effects of incidence on the interaction between passage vortices and tip-leakage flow in a low-speed linear cascade, based on detailed traverse measurements made with a five-hole pitot tube at six incidences. He showed clear occurrence of a high-loss region in the cascade passage due to strong flow separation originating from the pressure-side leading-edges as the incidence decreased. All such recent results related to the incidence effects can partly explain the mechanisms of the loss characteristics with incidence change in more detail. However, detailed flow/loss mechanisms within cascade passages at off-design incidence conditons have not been sufficiently explored yet, specifically in a quantitative manner; even very simple experimental data such as the streamlines or pressure distributions at the midspan passages, for example, have been scarce, although many computational results have been presented.

The primary objective of the present paper is to supply a set of detailed and quantitative information from which one can easily understand the cascade internal flow and loss mechanisms under various incidences and to which one can compare his computational results. The present test cascade is a low-speed linear cascade but will be able to simulate many of the flows occurring in real axial-flow turbine blade rows. The tip-leakage loss is not included in the present study.

TEST FACILITIES AND TEST METHODS

Low-Speed Linear Cascade Facility

Fig. 1 shows test section of the cascade used in the present study and is the same as that used in the previous studies [12]. Only the major specifications of the present (rotor) cascade are repeated here.

- Blade chord, C = 73.5 mm
- Axial blade chord, C_{ax} = 72.6 mm
- Blade pitch, S = 61.42 mm
- Aspect ratio, H/C = 1.37
- Solidity, C/S = 1.20
- Blade maximum thickness/C = 0.257
- Blade LE radius = 8.17 mm, TE radius = 4.08 mm
- Number of blades, N = 6
- Cascade camber angles, inlet = 49.8 deg
  outlet = −63.5 deg

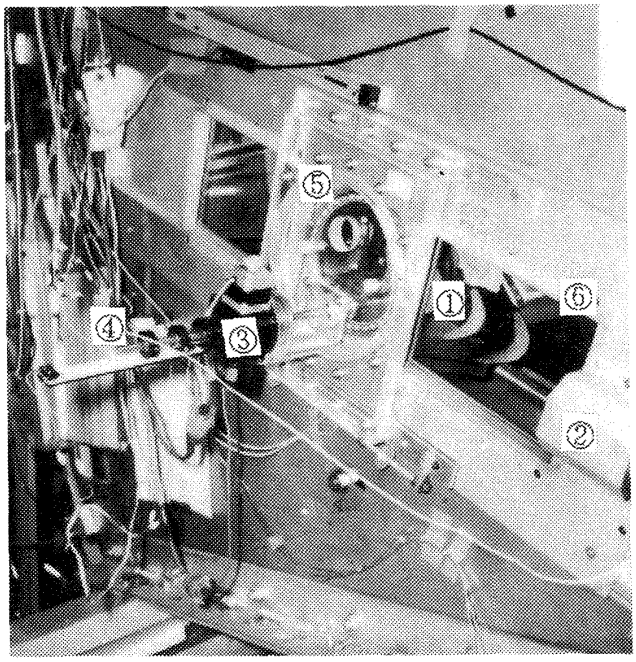

① Test cascade
② Pitchwise (X) gear
③ Radial and yaw traverse gear
④ Stem of sensor
⑤ Rotating disc
⑥ Tip-side endwall

Fig. 1 Test section of the cascade

- Design cascade turning angle = 113.3 deg
- Design flow angles, inlet = 43.6 deg
  outlet = −63.5 deg
- Design turning angle of flow = 107.1 deg

The cascade is a suction-type linear cascade with six blades with a large turning-angle, thick leading- and trailing-edges, low aspect-ratio and low solidity. Two inlet guide plates are installed upstream of the blades to change the cascade inlet flow angle (see Fig. 1 in [14]).

Traverse Measurements

Fig. 2 shows the setting angles of the inlet guide plates (IGP) and the traverse measuring planes (called S3-planes). The setting angle is indicated by $\theta_{y,g}$ or i_g where $\theta_{y,g}$ shows the angle measured from the cascade axial direction and i_g from the direction of the cascade inlet camber line. The periodicity of the cascade inlet and outlet flows was checked in advance to the present serial test with adjusting the inlet and outlet guide plates. It was found that the periodicity could not be always improved even with a special adjustment of the plates. The non-periodicity left, however, was negligibly small (typically as seen in Fig. 5) for the present

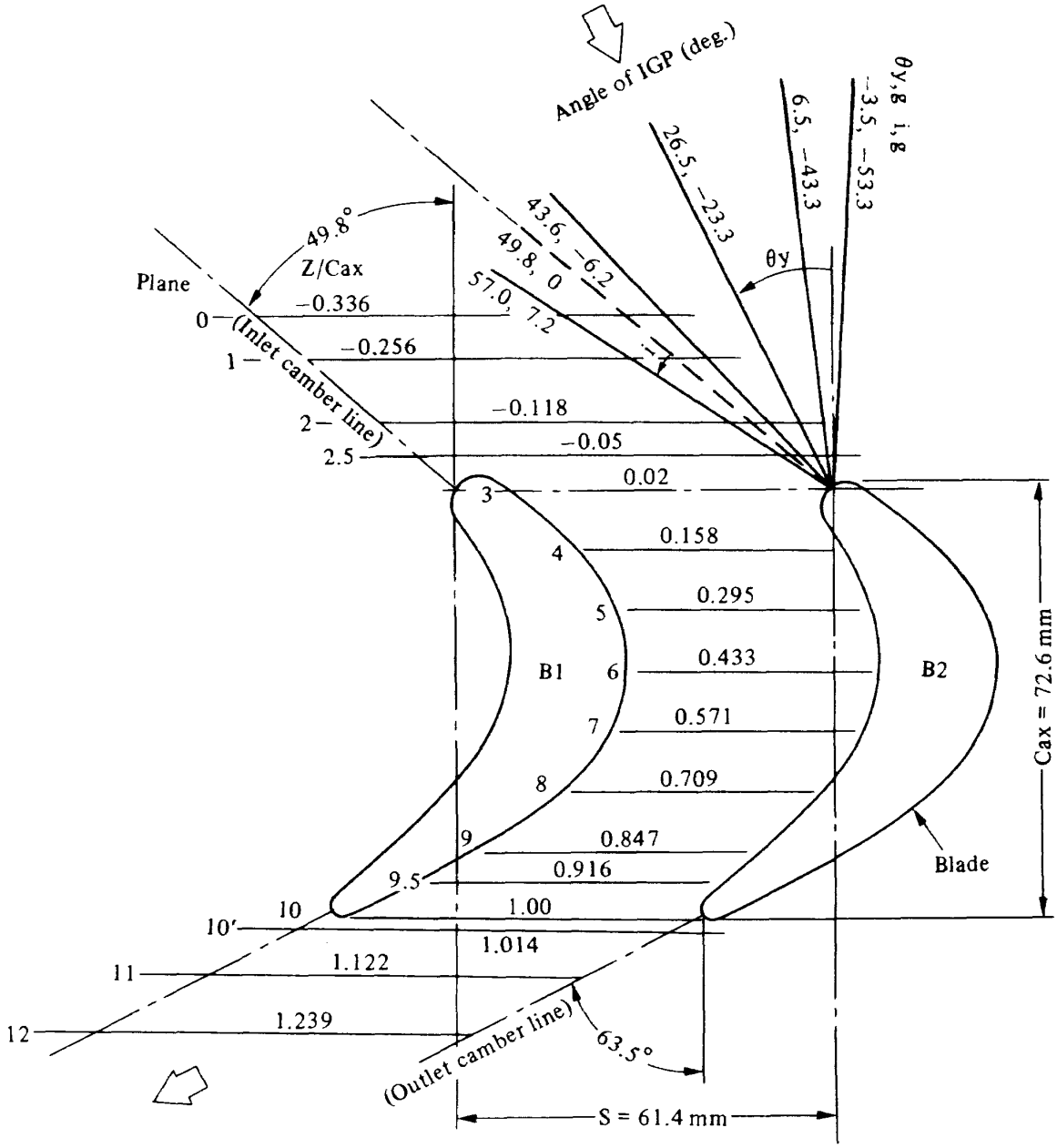

Fig. 2 Traverse S3-planes and test conditions

purposes. Therefore for each incidence test, the inlet guide plates were set in parallel to each other and the outlet ones were always fixed at the same position.

The test Reynolds number (Re, c) based on blade chord and mass-averaged outlet velocity at Plane 12 (Z/C_{ax} = 1.24) was about 1.8×10^5. This value is about the same as the typical Reynolds number used in Ainley's cascade data (2×10^5) but is lower about an order of magnitude than engine conditions. This does not mean the present cascade cannot simulate the flows in real machine. Unless the Reynolds number is extremely low, the difference to this extent is thought to be not so important as to change the flow mechanisms completely, although the Reynolds number effect has been still one of the most profound problems; in the author's opinion, what they detect as Reynolds number effects would result mainly or simply from the differences in the boundary layers, such as the thicknesses of inlet endwall boundary layer and of blade surface boundary layer, and in the turbulence level, when the test velocity was varied.

All of the above traverses were made using a miniature five-hold pitot tube with a head-size of 1.5 mm, the ratio of which to the cascade axial chord is about 48. Yaw direction of the pitot tube was kept fixed during the measurement at each plane and the absolute flow directions were determined with calibration data obtained in advance.

EXPERIMENTAL RESULTS AND DISCUSSION

Cascade Inlet and Outlet Flow Conditions

Fig. 3 shows the velocity profiles at the cascade inlet Plane 0. The relationship between the inlet boundary layer parameters obtained at Plane 1 and the setting angle of the inlet guide plates (IGP), $\theta_{y,g}$, was shown in Fig. 3 of the previous paper [13]: The endwall boundary layer on the tip-side endwall was a little thicker than that on the hub-side. The shape factor of

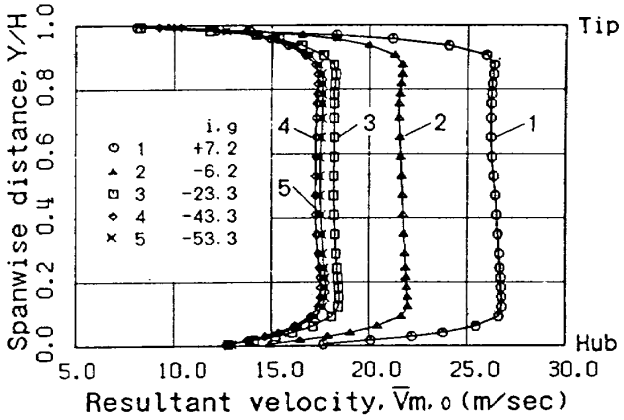

Fig. 3 Pitch-averaged inlet velocity profiles at S3-plane 0 for various test incidences

the tip-side boundary layer varied from 1.37 to 1.60 for $\theta_{y,g}$ = −3.5 to 43.6 degrees and 1.88 for $\theta_{y,g}$ = 57.0 degrees. The hub-side shape factor varied less, from 1.21 to 1.33 depending on the incidence. This indicates the tip-side inlet boundary layer to be in a transitional state (typically the value is 1.7) from turbulent (1.37) to laminar (1.88), and the hub-side layer to be always fully turbulent (nearly 1.3).

Fig. 4 shows the yaw angle distribution throughout the cascade for three incidences. As shown here, and partly recognizable in Fig. 5, the inlet flow direction at the most upstream Plane 0 (Z/C_{ax} = −0.336) that is not far upstream from the cascade leading-edge, does not necessarily coincide with the direction of the guide plates. The flow has already been influenced by the cascade. As was shown in [13], the inlet flow direction (mass-averaged value) at Plane 1, for example, is 7 to 12 degrees smaller than the setting angle of the inlet guide plate, corresponding to $\theta_{y,g}$ of −3.5 to 57.0 degrees (or $i_{,g}$ of −53.3 to 7.2 degrees).

The outlet yaw angles obtained at Plane 12 indicate that the effect of the passage vortices clearly appears in the spanwise distribution. The effect gets stronger with increase of the incidence (i.e., increase of the cascade turning). The mass-averaged values, however, were nearly constant between −60.4 and −60.7 degrees regardless of the incidence change.

Incidence Effects on Midspan and Downstream Flows

Fig. 5 shows the midspan flows for five incidences. The vectors showing the midspan flows, W, correspond to the vectors of resultant velocities projected onto the blade-to-blade plane (called S1-plane) parallel to the endwall. In each of the figures, secondary flows and total pressure loss contours obtained at downstream Plane 12 are also shown. The secondary flow vector V_s was defined as the velocity component normal to the local midspan flow at the same pitchwise location. Note that to clearly show the secondary flows, the scale of V_s is increased to ten times that of W. The major results are as follows:

As the incidence decreases toward negative values, flows near the blade pressure surface tend to easily separate from the blade leading-edges. The separated areas are illustrated as the areas with very small velocities. If back flows exist, they were not detected by the present pneumatic probe. The reattachment point (or region) of the separated flow on the pressure surface can also be recognized. It should be noted that the midspan flows downstream of the trailing-edge are not influenced at all by the incidence change. Within the cascade passage, the flows near the suction surface are generally much accelerated compared to those near the pressure surface. As the incidence decreases, the difference between the velocities at the suction side and those at the pressure side gets smaller and the flows tend to be uniform in the pitchwise direction, outside the separation region. The overall flows are much accelerated due to the blockage effect of the flow separation.

The downstream flows in Fig. 5 show that the passage vortex generated in the cascade is very strong at the maximum incidence ($i_{,g}$ = 7.2 degrees). With the decrease of incidence, it gets rapidly weaker. The associated loss, i.e., the loss due to the low-energy fluids accumulated by the vortex in the wake region, therefore, decreases. However, at the incidences of less than −23.3 degrees, the wake expands from the blade pressure side to the free stream region due to the leading-edge separation. At the minimum incidence tested, the wake dominates most of the cascade passage, driven by new secondary flows near the midspan. The generation of the new secondary flows will be seen later in Fig. 12.

Incidence Effects on Midspan Static and Total Pressures, and Velocity

Fig. 6 shows the distributions of static pressure, total pressure loss and velocity at the midspan for four incidences, superimposed on vectors W. The static pressure contours CP_s show that as the incidence decreases, the blade loading in the front part of the cascade passage decreases. The front part of the cascade is very sensitive to the incidence variation, but the rear part is not.

The total pressure contours CP_t show that there exist two regions of loss generation: One is located on the suction surface where the boundary layer starts to develop rapidly from a little upstream of the cascade throat, due to adverse pressure gradient in this region as seen in CP_s. This loss seems to be insensitive to incidenc change. The other is located near the pressure side, where the flows separate from the blade leading-edge, even at the maximum incidence tested, due to the small region on the pressure surface with adverse pressure gradient. The separation causes large pressure loss.

The velocity contours CV_m clearly reveal two low-velocty regions which indicate the suction-side boundary layer development and the pressure-side flow separation. The separation seen at the maximum incidence was visualized by atmospheric dust accumulated on the pressure surface after the long run of the serial tests and also by oil-smoke trace; the smoke showed a strong spanwise flow passing the pressure surface near the leading-edge from the endwall corner to the midspan.

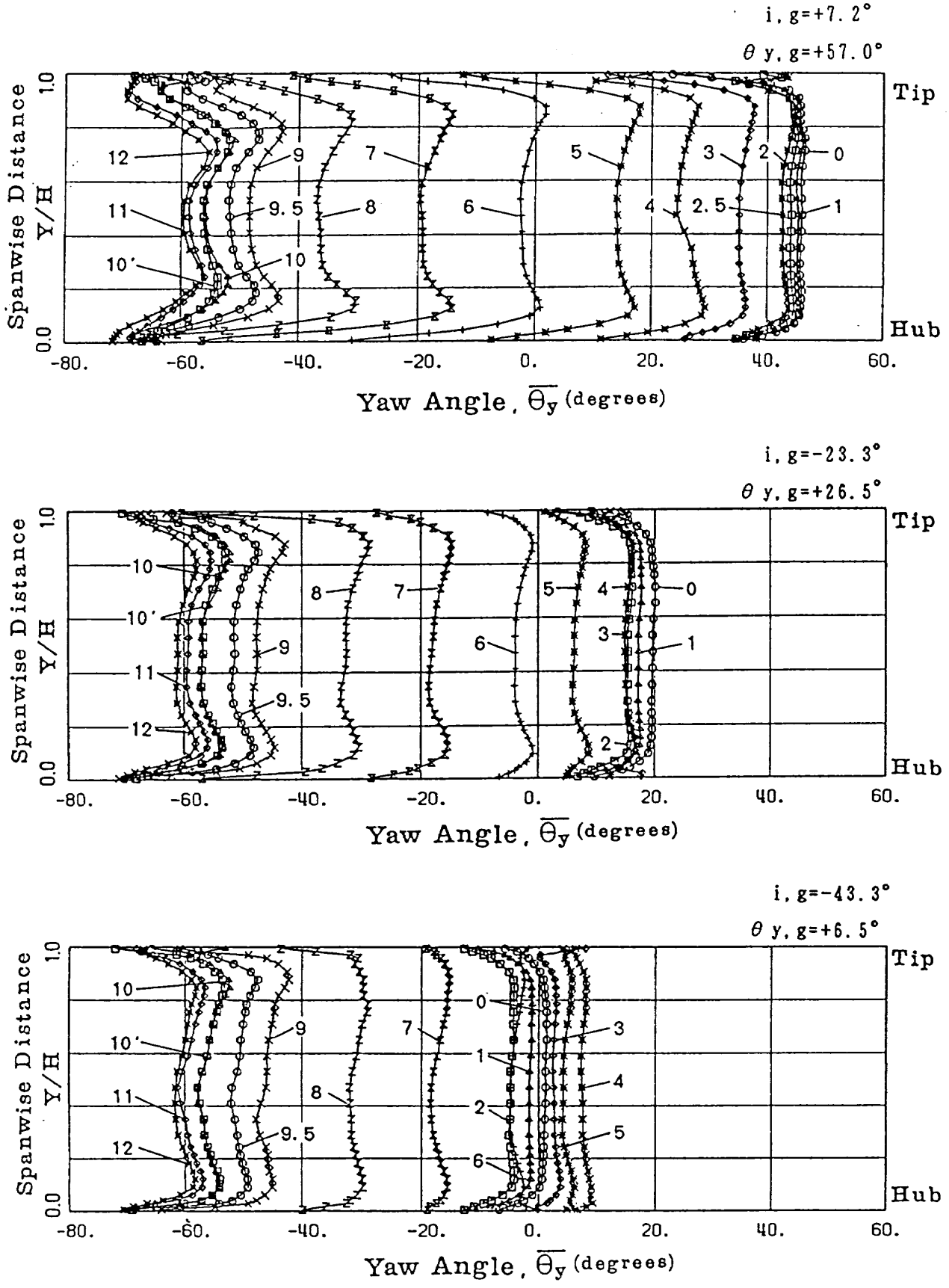

Fig. 4 Pitch-averaged yaw flow angles at various S3-plane for three inlet guide angles

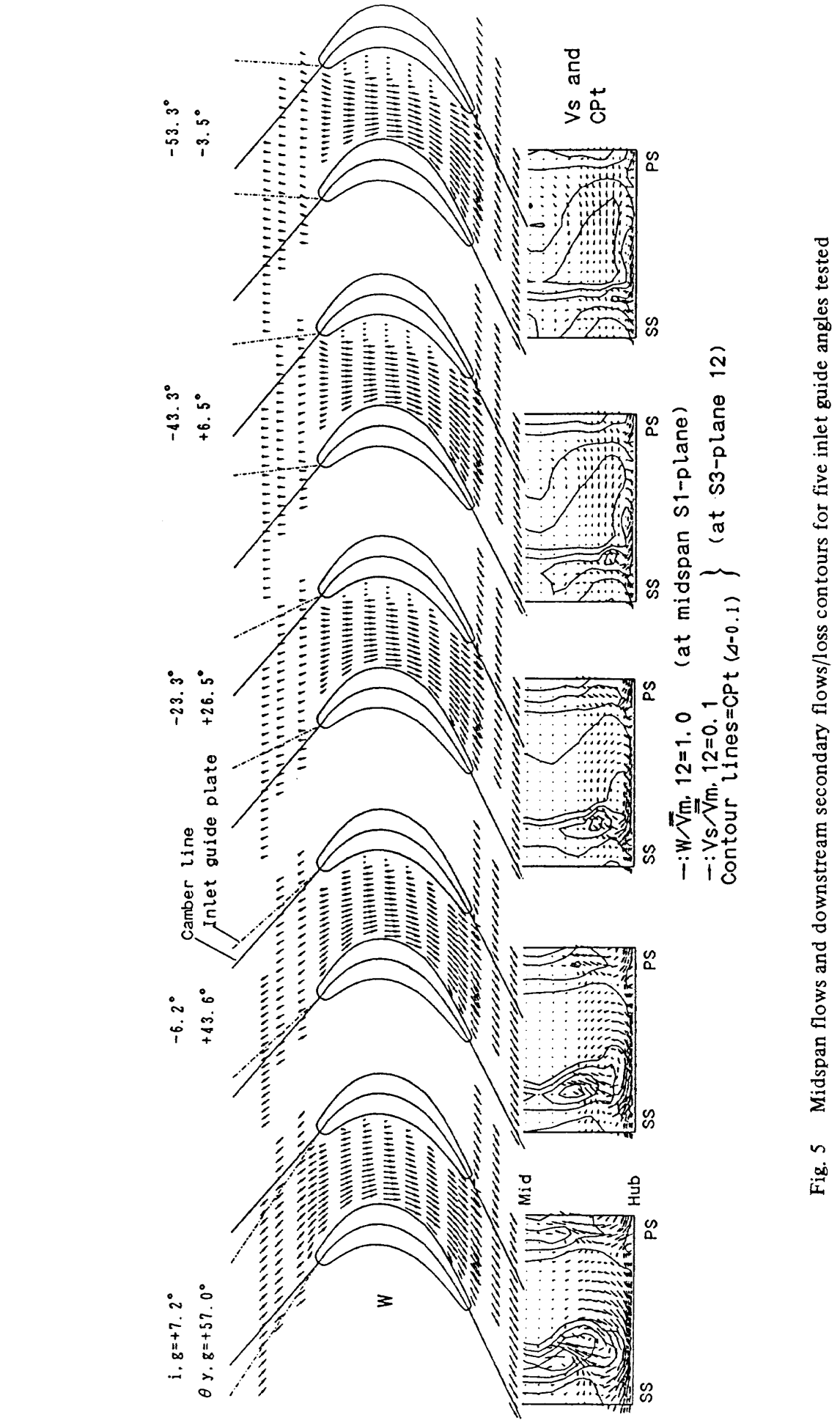

Fig. 5 Midspan flows and downstream secondary flows/loss contours for five inlet guide angles tested

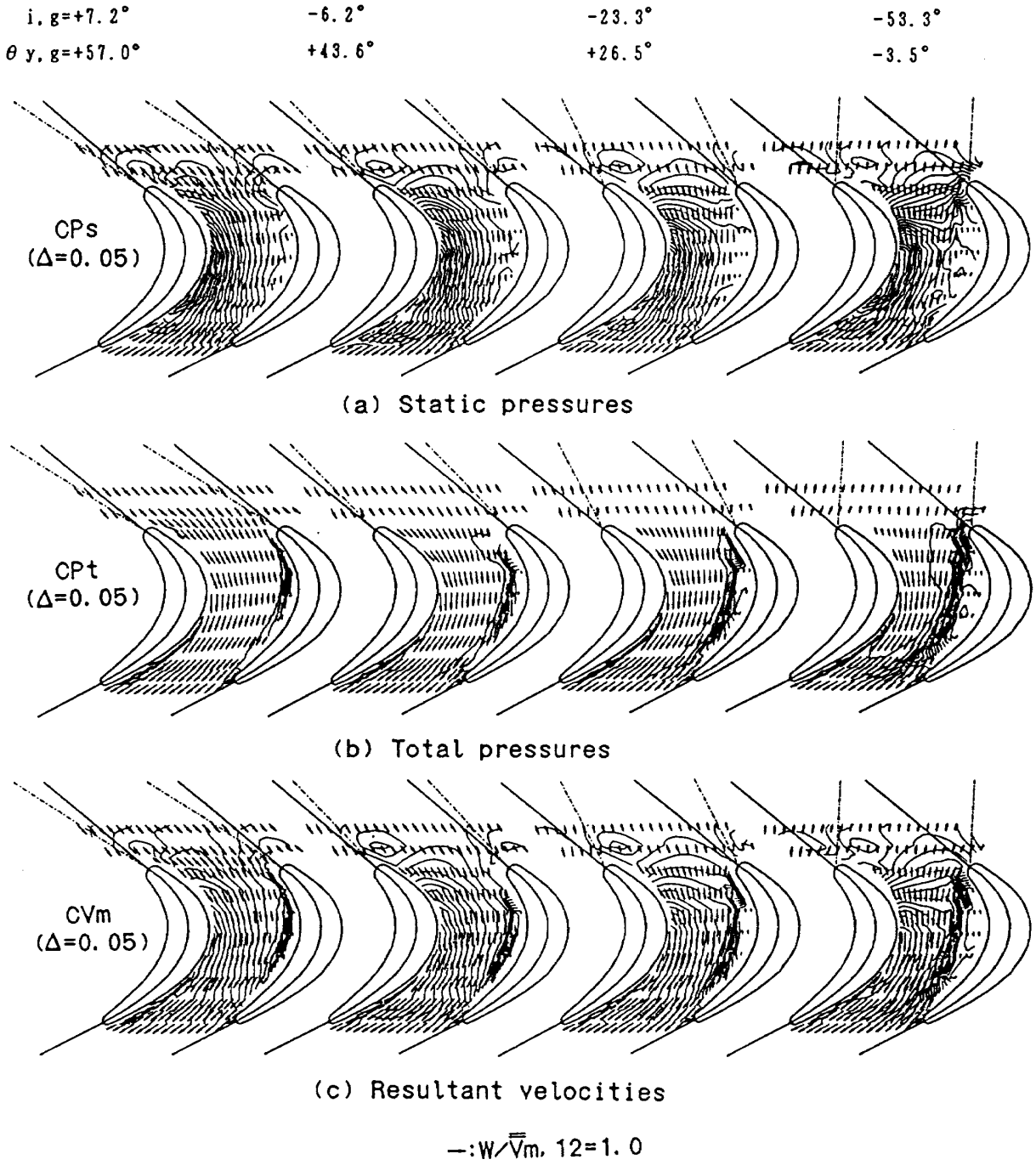

Fig. 6 Three types of contours of static pressures, total pressures and velocity at midspan S1-plane with vectors W for four inlet guide angles

Incidence Effects on Endwall Flow Vectors

Fig. 7 shows the effect of incidence on the endwall flows obtained at the blade-to-blade plane closest to the hub endwall, i.e., at 1.2 percent of the blade span away from the endwall. As the incidence increases, the endwall flows within the cascade passage migrate more strongly toward the blade suction surface, as often seen in flow visualization results. This is caused by the increased pitchwise pressure gradient particularly in the front half of the cascade passage as seen in the previous CP_s contours, due to the increased turning of the cascade flow. At the maximum incidence tested, most of the vectors between Plane 8 (Z/C_{ax} = 0.7) and Plane 10 (Z/C_{ax} = 1.0), except in a small region near the pressure surface, face almost normal to the axial direction. The endwall flows at the farthest downstream Plane 12 (i.e., Z/C_{ax} = 1.24), however, are insensitive to in-

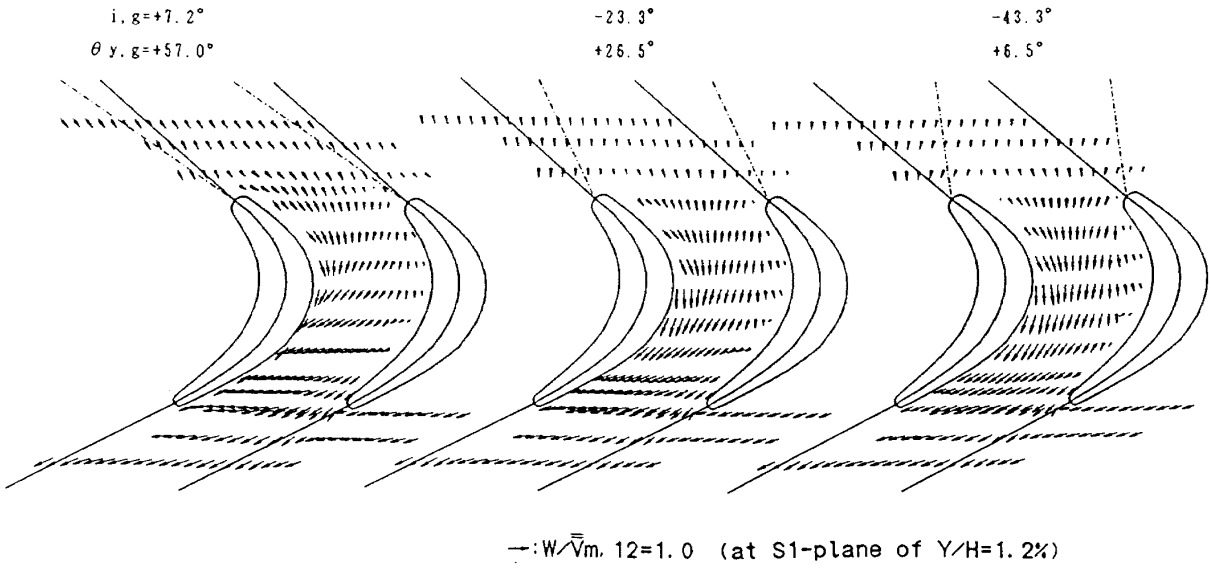

Fig. 7 Hub endwall flow vectors for three inlet guide angles

cidence variation. This insensibility downstream was seen also in the midspan flows (Fig. 5). Compared to the area of flow separation seen at the midspan, the separation area near the endwall seems to be reduced.

Incidence Effects on Static Pressures near Endwalls and near Blade Surfaces

Fig. 8 shows a three-dimensional representation of the static pressure distributions near the tip endwall (at 1.2 percent span from the tip endwall), near the blade suction surface and at the cascade exit Plane 10 (Z/C_{ax} = 1.0). The distributions are again superimposed with W and V_s to make the results easily understood. As seen from the tip endwall flow vectors at the maximum incidence, some of the flows near the pressure-side leading-edge nearly stagnate, while this will not be seen in the hub endwall flows shown later in Fig. 9, although both endwall flows were measured at the same distance from each wall. The stagnation flows are thought to appear because the tip-side endwall boundary layer was thicker than the hub-side and so the measuring plane of the tip endwall flows penetrates deeper into the endwall boundary layer than that of the hub endwall flows. Thus the endwall flow patterns depend strongly on the location of measuring plane, or on the cascade boundary layer thickness. Except for this difference, the general tendency of the pressure distribution to vary with incidence variation is similar on both endwalls, and also similar to the midspan static pressure distribution as seen previously (Fig. 6a). A clear difference of the endwall distribution from the midspan one can be found at the maximum incidence where a minimum pressure peak occurs apart from the suction surface in the rear half of the cascade passage due to the strong passage vortex. As the incidence decreases, the minimum peak point moves upstream and close to the suction surface.

At the cascade exit, on the other hand, the static pressures are far from uniform in the spanwise directions at the maximum incidence due to the strong passage vortices, while they are fairly uniform at other incidences except near the suction surface/endwall corners. The centers of the vortices nearly coincide with the static pressure minimum peaks. The suction surface pressure distributions can be seen to be affected by the passage vortices with rolling-up inlet endwall fluids on the surface, especially at the maximum incidence.

Fig. 9 shows the static pressure distributions near the hub endwall (1.2 percent span from the hub wall), and near the blade surfaces. Each figure includes vectors and streaklines or lines of particle path, which resemble to the oil- or ink-

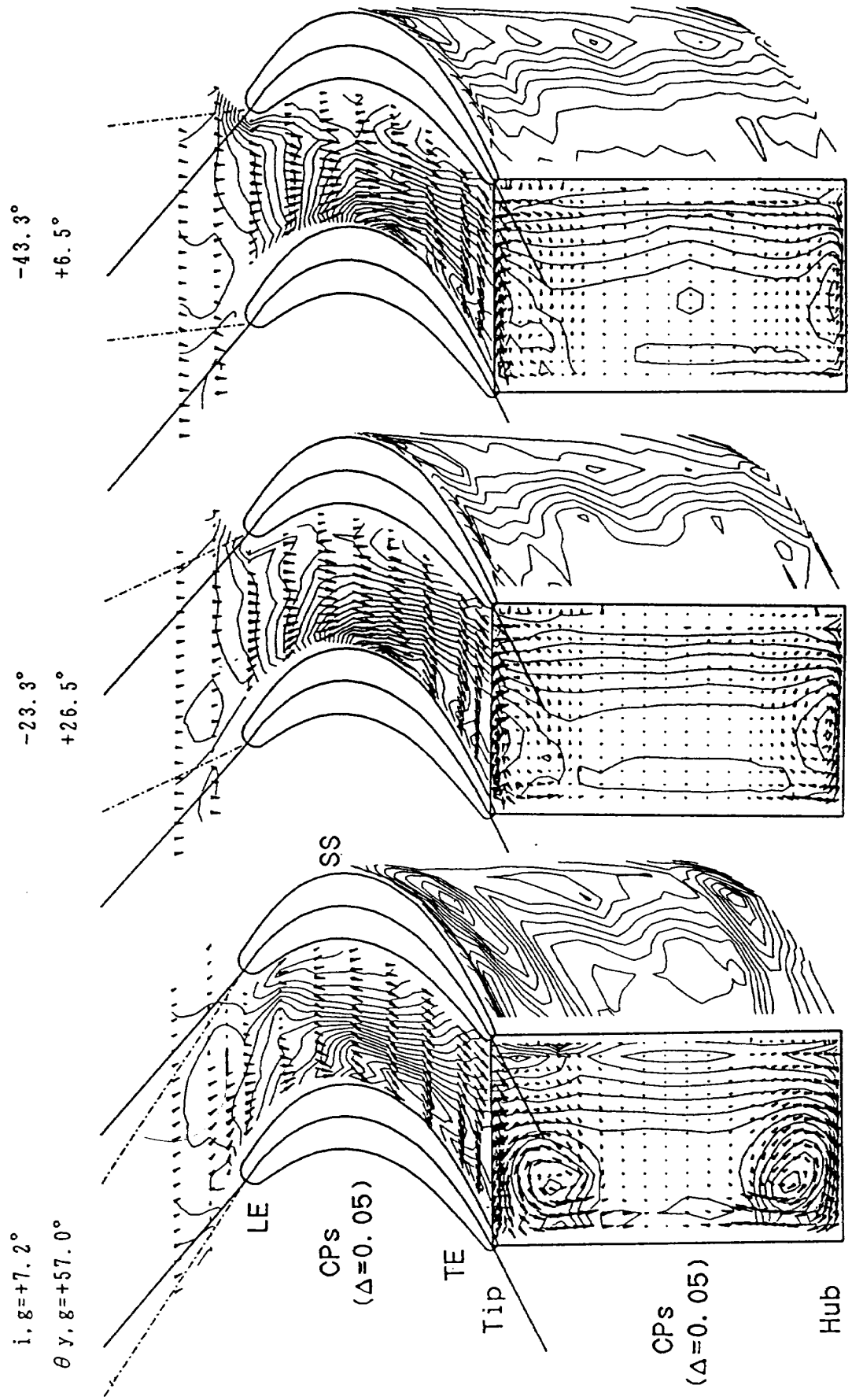

Fig. 8 3D representation of static pressure contours with vectors W and Vs for three inlet guide angles

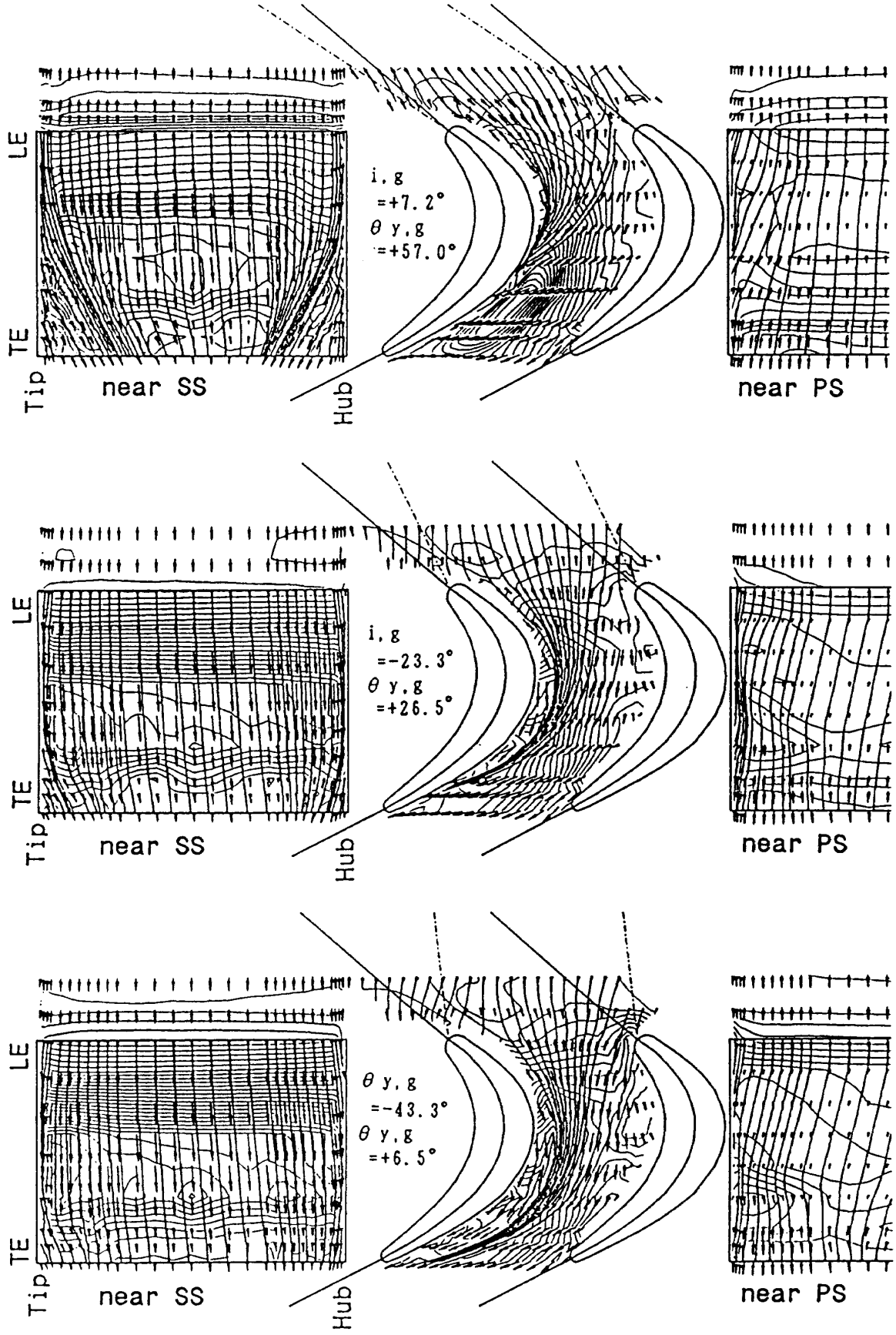

Fig. 9 Static pressure contours, streaklines on SS and on hub-endwall with vectors W (on hub casing) and Vz (on SS) for three inlet guide angles

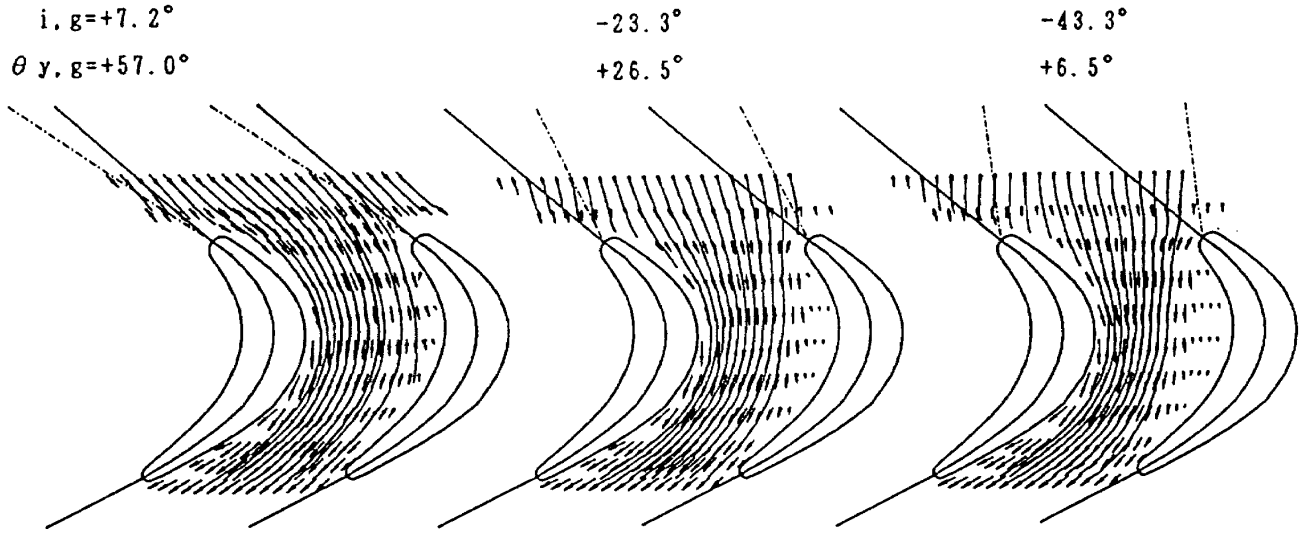

(a) At midspan plane (IY=15, Y/H=50%)

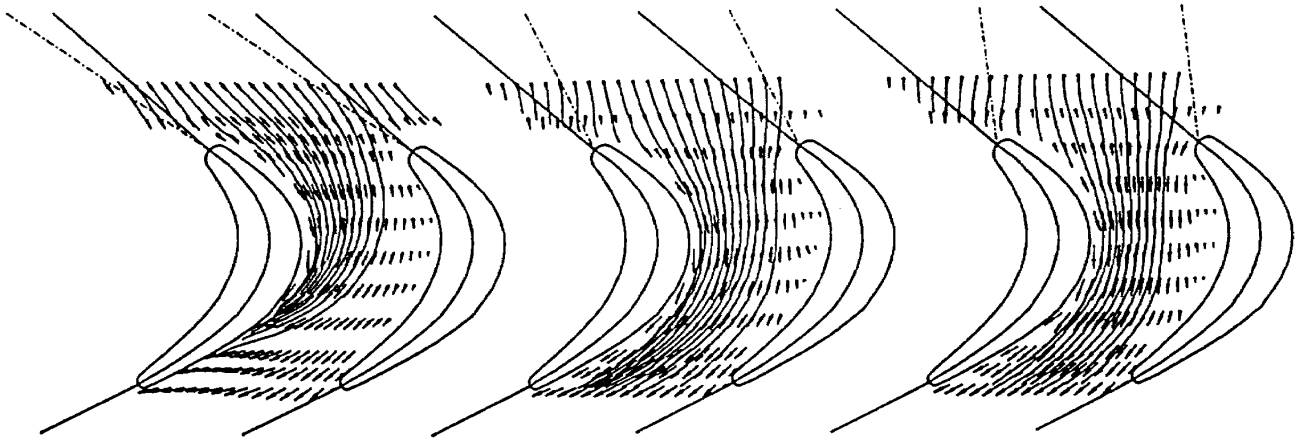

(b) At plane near hub endwall(IY=3, Y/H=3.6%)

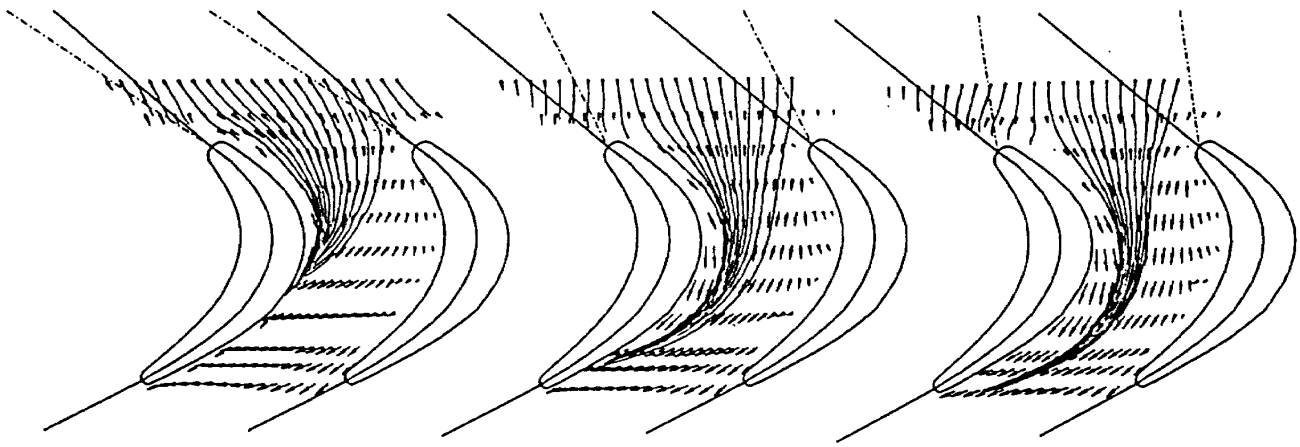

(c) At plane closest to hub endwall(IY=1, Y/H=1.2%)

Fig. 10 Streaklines of inlet flows on three S1-planes for three inlet guide angles

flow visualizations that were often made on cascade endwalls and on blade surfaces by many workers [2, 3, 4, 6, 9, 10, 15, 16, 17]. The minimum pressure peak can be seen on the hub endwall, too, at the maximum incidence and is located in the region of newly generated endwall boundary layer after the inlet boundary layer fluids are completely skewed as shown by the streaklines. The streaklines exhibit the rollup from the endwall decreases very rapidly. It is interesting to note that all the inlet endwall streaklines. The streaklines exhibit the rollup of the inlet endwall boundary layer fluids from the wall onto the blade suction surface. This quantitative flow visualization clearly shows that as the incidence decreases, the height of the roll-up from the endwall decreases very rapidly. It is interesting to note that all the inlet endwall streaklines tend to gather into one line with keeping a relatively wide space between the line and the blade suction surface. In this space, a vortex (Hs) is considered to exist without diminishing, as will be seen later in Figs. 11 and 12.

Incidence Effects on Midspan and Endwall Streaklines

Fig. 10 shows the effects of incidence on the streaklines on three blade-to-blade planes obtained at the midspan and close to the hub endwall. The figure can be considered to demonstrate roughly the skewness of the cascade so-called 'streamlines'. On the midspan plane, the streaklines pass through the passage nearly parallel to each other. The streaklines close to the blade suction surface, however, are not parallel to the suction surface of the rear half, due to the boundary layer development on the surface. This experimental result is different from what is obtained by an inviscid streamline computation (e.g., in Fig. 12 of [18]); on the rear half of the suction surface where adverse pressure gradient exists, a boundary layer can easily develop possibly with flow separation and then viscous effects cannot be neglected. The streaklines are highly skewed, only when they approach the endwall very closely; at the maximum test incidence, the streaklines both at 1.2 and 3.6 percent of span are highly skewed, while at the negative incidences, those only at 1.2 percent span are significantly skewed.

The actual streaklines do not always remian on one blade-to-blade plane and generally move in three-dimensional space. Fig. 11 gives the pitch angle contours of the flows at 3.6 percent span away from the hub endwall. The solid lines indicate that the flows are rolling up from the hub in the spanwise direction. A relatively large region with solid lines (denoted by A) exists along the blade suction surface at the maximum incidence and moves roughly up to 1/3 – 1/2 the

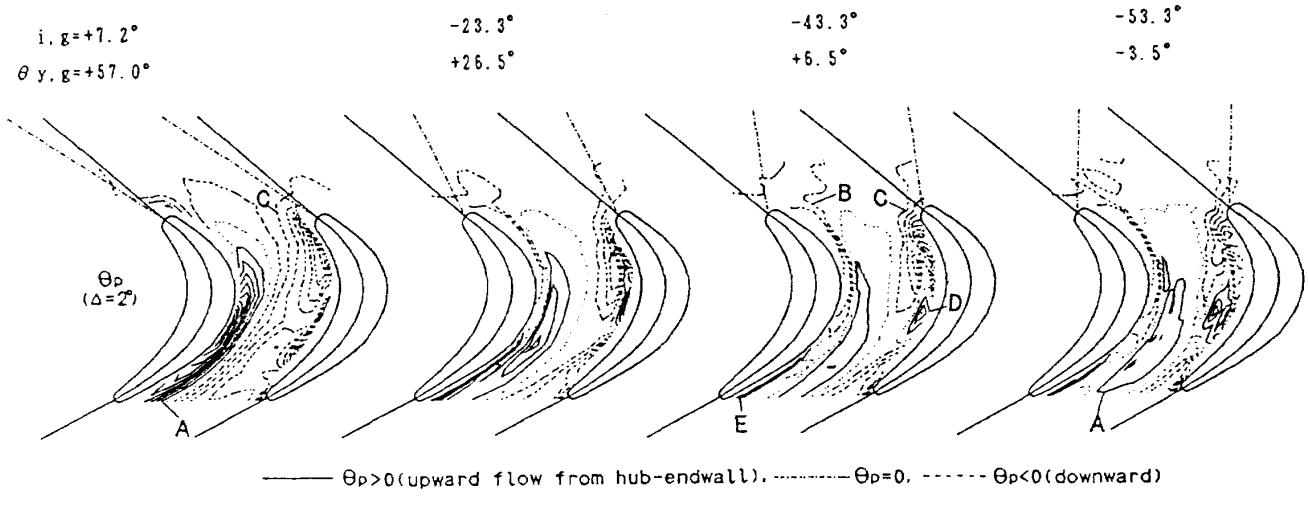

Fig. 11 Pitch angle contours near hub endwall (Y/H = 3.6%) for four inlet guide angles

width from the suction surface at the minimum incidence. An area with dotted lines (B) can be seen between the solid line area described above and the suction surface for all test negative incidences, which indicates an existence of rolling-down flows toward the hub. Near the blade pressure surface, rolling-down flows (C) also exist. Therefore, two contra-rotating vortices possibly exist at both sides of the area indicated by solid lines (A). A small area of rollup flows (D) is also recognized to exist in the region C. Note that at negative incidences, a very thin area with solid lines (E) remains very close to the suction surface downstream of the cascade throat, showing that there is a rollup flow at the suction surface/endwall corner.

Incidence Effect on Development of Secondary Flows and Losses

Fig. 12 shows details of the development process of some secondary vortices and losses under various incidence conditions. Some of the traverse planes are chosen and only the hub-side halves of them are presented here. Special attention is given to the identification of the passage vortex, the pressure-side and suction-side legs of the horseshoe vortex, and other new secondary flows caused by the leading-edge separation.

At cascade inlet Plane 3 (Z/C_{ax} = 0.02), both of the legs (Hs and Hp) can be seen under all incidence conditions. The point of intersection between Hs and Hp, indicated by an arrow, moves from the suction side to the pressure side as the incidence decreases. At Plane 5 (Z/C_{ax} = 0.3), it is difficult to distinguish between Hp (caused mainly by the spanwise pressure gradient) and the passage vortex (caused mainly by the pitchwise pressure gradient), since both vortices rotate in the same direction. However, at an incidence of less than −43.3 degrees, the vortex seen at the pressure side is thought to be attributed largely to the Hp, since the pitchwise pressure gradient is not so large to cause the passage vortex, as was seen in Fig. 9. The merging of the two vortices at the entrance region thus depends largely on the cascade incidence. At the cascade entrance region, Bario et al. [18] showed the absence of Hp of the horseshoe vortex in their highly loaded cascade with a turning of 125 degrees, while Langston [3] and Marchal and Sieverding [4] showed the eistence of Hp as well as Hs in their moderately loaded cascades. The votex Hs, on the other hand, can be clearly recognized at Plane 5 for all text negative incidences. For incidences of less than −43.3 degrees, Hs can be recognized even at the cascade exit Plane 10. Close inspection of the endwall flows reveals that at all of the planes downstream from Plane 9, the flows closest to the endwall (i.e., at IY = 1) always move from the pressure side to the suction side, even if the contra-rotating vortices (Hs and Hp) exist over these endwall flows.

At the maximum incidence tested, the strength of the passage vortex increases with the axial distance Z/C_{ax}, and the center of the vortex gradually separates from the endwall. At the other incidences, however, the center is nearly fixed at a constant span. Leading-edge separation loss appears at Plane 5 along the blade pressure surface. The leading-edge separation plays a major role in the overall cascade loss at negative incidences. The loss begins to diffuse into the mid-passage from the pressure side to the suction side. In this diffusion process, free-stream high-energy fluids are first fed to the endwall regions of the separated flow, due to secondary flows toward the pressure surface/endwall corner. Some of the fluids are then driven into the separated region away from the endwalls by new secondary flows that rollup onto the pressure surface.

Incidence Effects on Total Pressure Losses near Endwalls and Blade Suction Surface

Fig. 13 shows three-dimensional representations of the loss contours near the tip-side endwall and near the suction surface, with

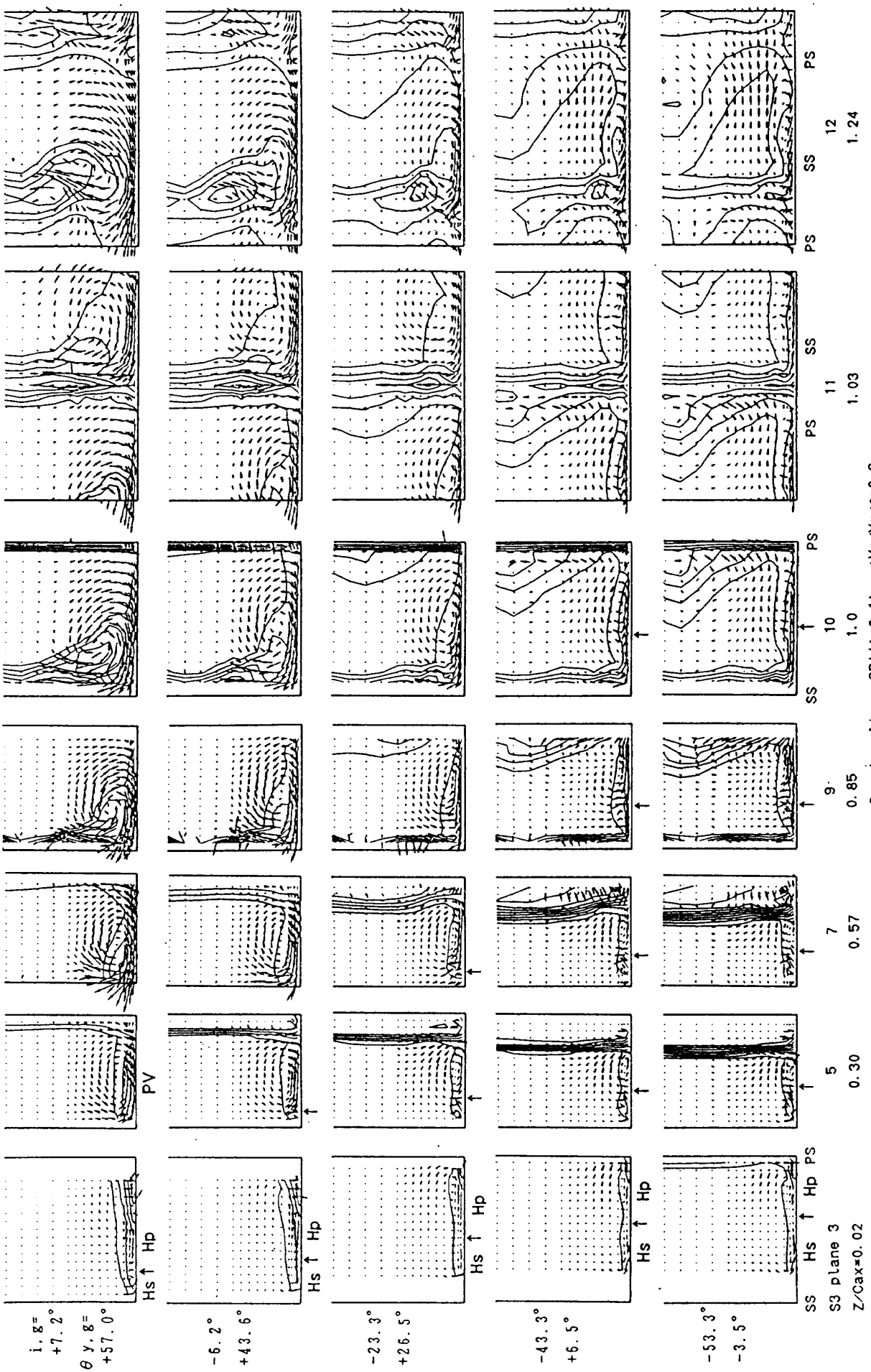

Fig. 12 Development of secondary flows and total pressure losses at various S3-plane (Hub side halves are presented)

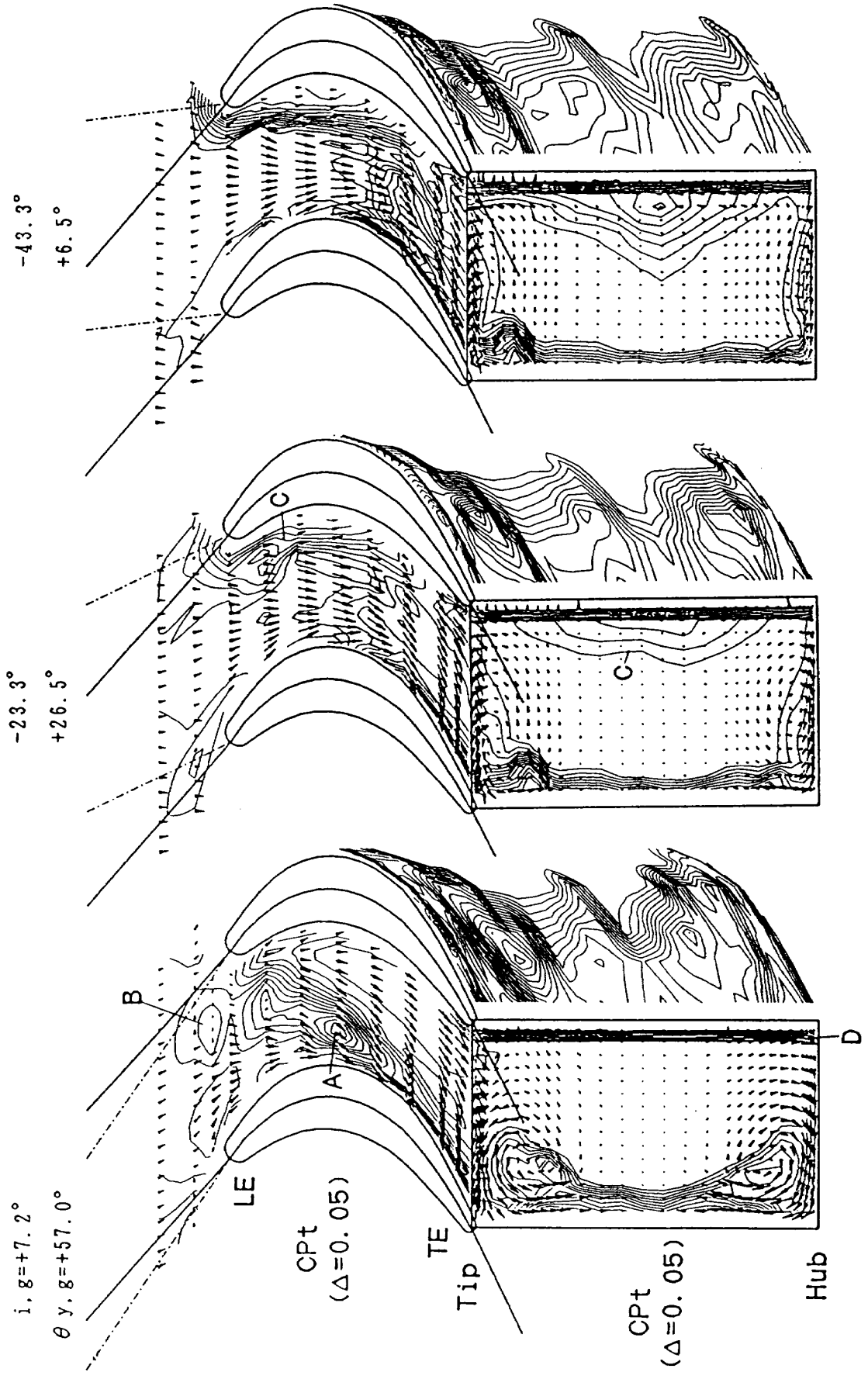

Fig. 13 3D representation of total pressure loss contours with vectors W and Vs for three inlet guide angles

superimposed vectors W and V_s. The loss distribution at the cascade exit plane illustrates the net cascade loss which is generated in the cascade passage between Planes 0 and 10. Development of the loss near the endwalls is more complicated than that at the midspan shown in Fig. 6(b): At the maximum incidence, a high-loss region with a peak (denoted by A) extends from the pressure side of the leading-edge to the rear suction surface of adjacent blade. Another loss peak (B) is located upstream of the leading-edge. At the negative incidences, the loss (C) due to flow separation from the blade leading-edge is transported to the rear half of the suction side over the endwalls. This high-loss region seems to extend around the leading-edge more widely near the endwalls than at the midspan (Fig. 6b).

The cascade exit loss contours show that at the maximum incidence, the loss accumulated on the blade suction surface results from the low-energy fluids which migrate from both endwalls, and from the boundary layer loss (profile loss) which developed on the surface. As the incidence decreases, however, amount of the low-energy fluids migrating from the endwalls decreases, and the loss on the suction surface results mainly from the boundary layer loss (profile loss). Looking at the loss on the pressure surface, on the other hand, a boundary layer can hardly develop on this surface; only the wake loss (D) is seen at the maximum incidence. When the incidence decreases to negative values, a large loss (C) is generated over the pressure surface, due to the flow separation from the blade leading-edge and becomes one of the main cascade losses.

Fig. 14 shows the loss contours near the hub-side endwall and near the suction surface. To the loss contours, some streaklines starting upstream of the cascade were added in order to show a clear relation between the flows and the losses generated near the cascade solid surfaces. At the maximum incidence, the inlet flows have already been swept out completely from the endwall at about half axial chord and are accumulated on the suction surface. The accumulated flows moves to about 1/4 span away from the endwall at the trailing-edge. On the endwall after the inlet flows were swept out, a loss peak appears due to high-loss fluids generated by the strong passage vortex. As the incidence decreases, the inlet endwall fluids are not completely swept out and remain on the endwall farther downstream. The endwall loss appears to consist of the loss caused by the corner flow (Hs) along the suction surface, the loss caused by the passage vortex mainly on the rear part of the endwall, and the loss caused by the leading-edge flow separation along the pressure surface.

Quantitative Flow Visualization

Fig. 15 shows streaklines which were analyzed as if oil-dots or oil-smoke were injected from all traverse measuring points. Since some of the streaklines of the inlet flows starting upstream of the cascade have already been discussed, attention here is focussed on the effect of incidence on the rest of the streaklines: In the figures (c), for example, it can be seen that new boundary layer flows, which contain the fluids coming from the midspan side, arise downstream of the streaklines of the inlet flows and migrate toward the suction side. As the incidence decreases to -23.3 and -43.3 degrees, the new boundary layer fluids migrate less intensely toward the suction side and cannot reach the blade suction surface beyond an accumulation line (or region) of inlet boundary layer fluids. Between the suction surface and the accumulation line, a corner flow (Hs) possibly exists.

Incidence Effects on Blade Loading at Tip

Fig. 16 shows the effect of incidence on blade loading (or blade surface static pressure) distributions at the blade tip section, which were obtained from tip-endwall static pressure measurements (see [14] for details). A comparison between the static pressures at the midspan (Fig. 6a) and near the tip (Fig. 8) or the hub

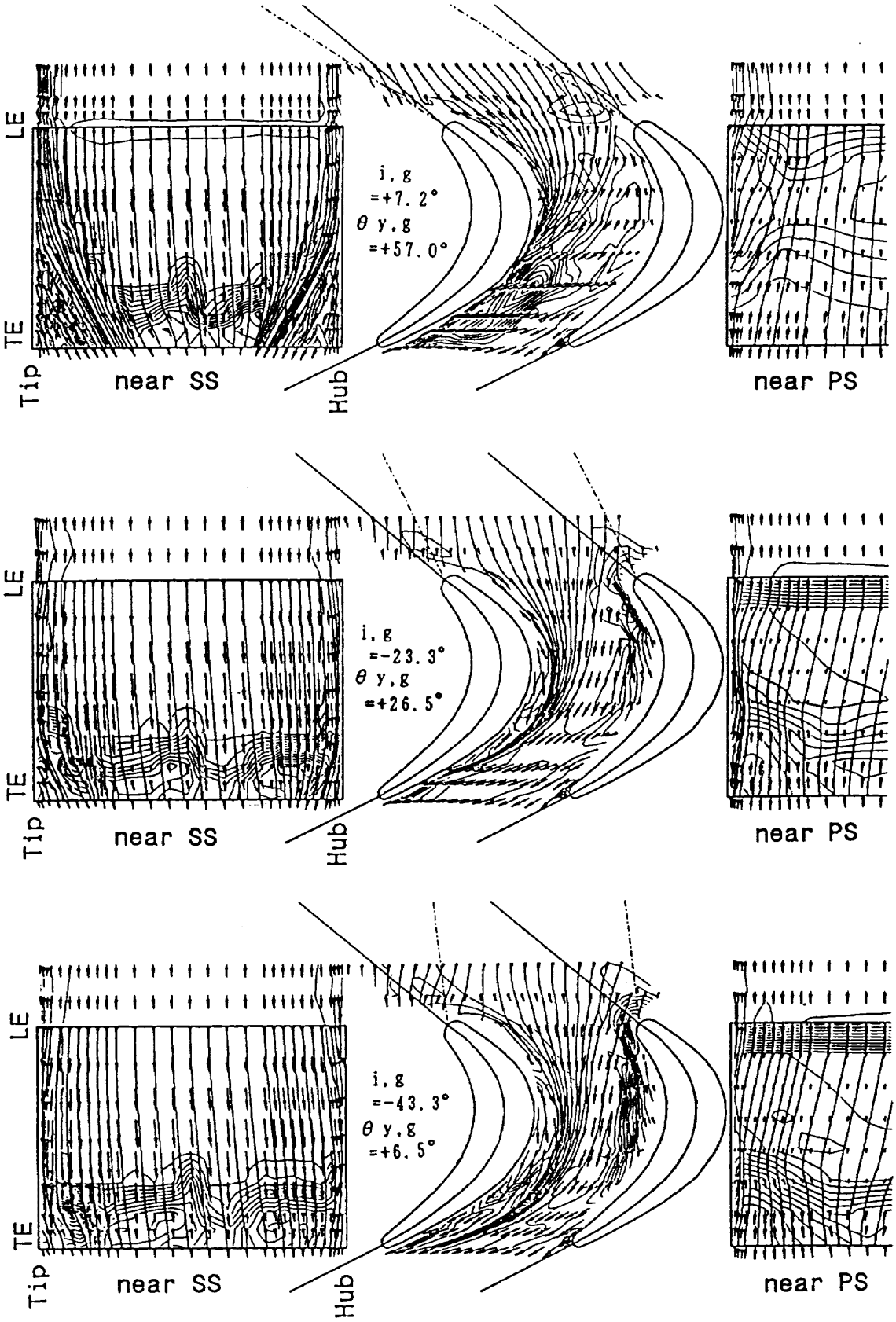

Fig. 14 Total pressure contours, streaklines on SS and on hub-endwall with vectors W (on tip casing) and Vz (on SS) for three inlet guide angles

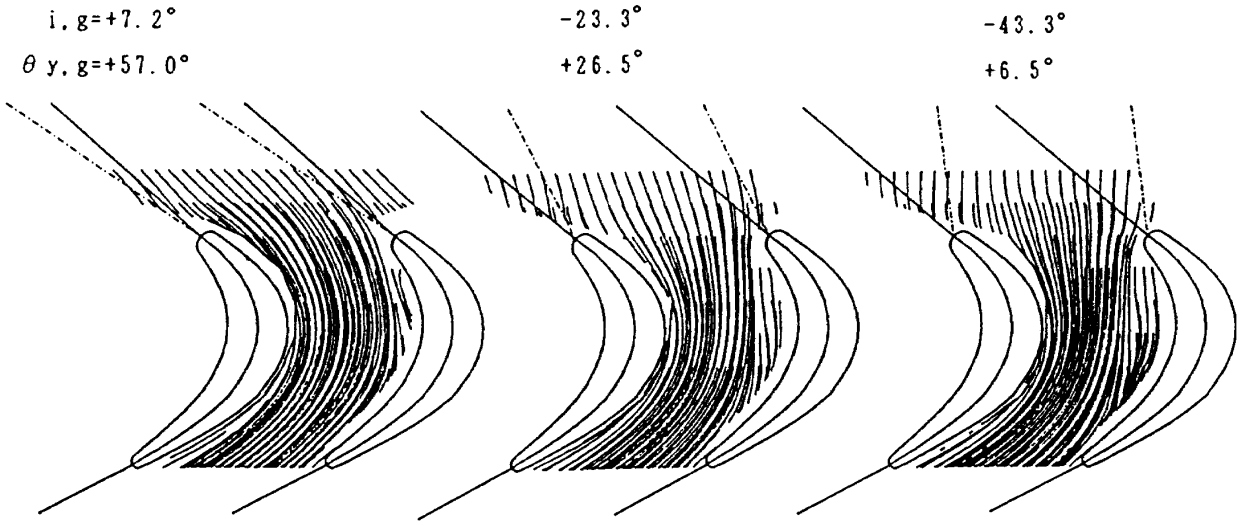

(a) At midspan plane(IY=15, Y/H=50%)

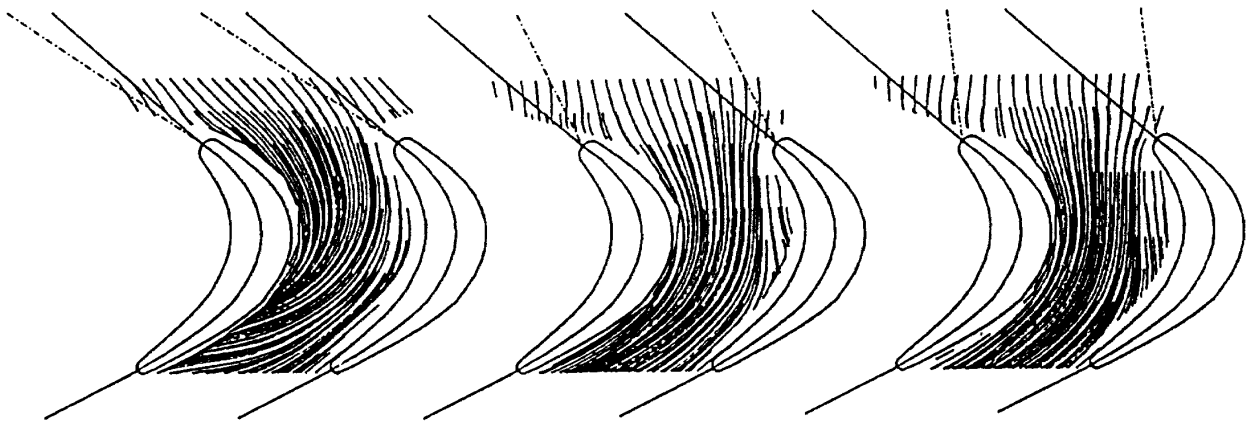

(b) At plane near hub endwall(IY=3, Y/H=3.6%)

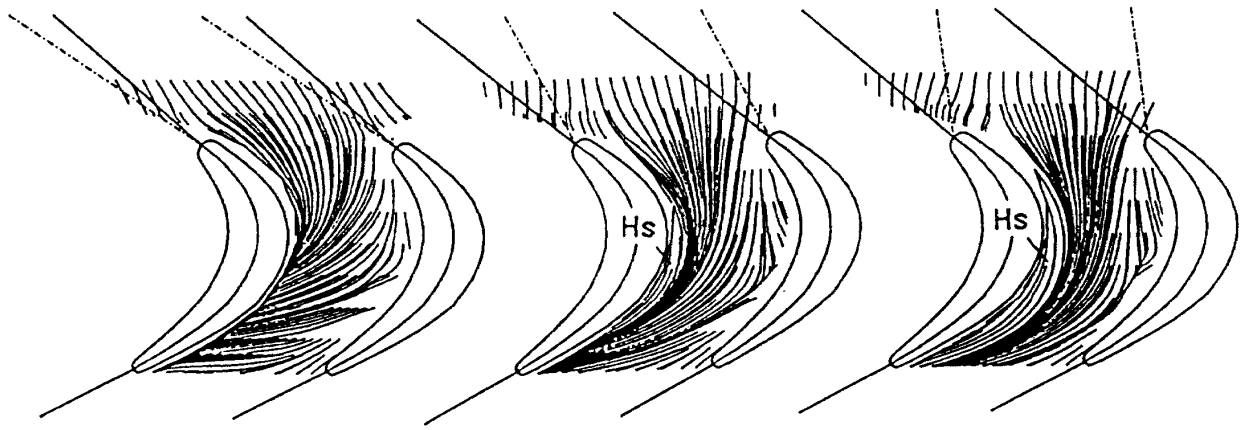

(c) At plane closest to hub endwall(IY=1, Y/H=1.2%)

Fig. 15 Streaklines at three S3-planes

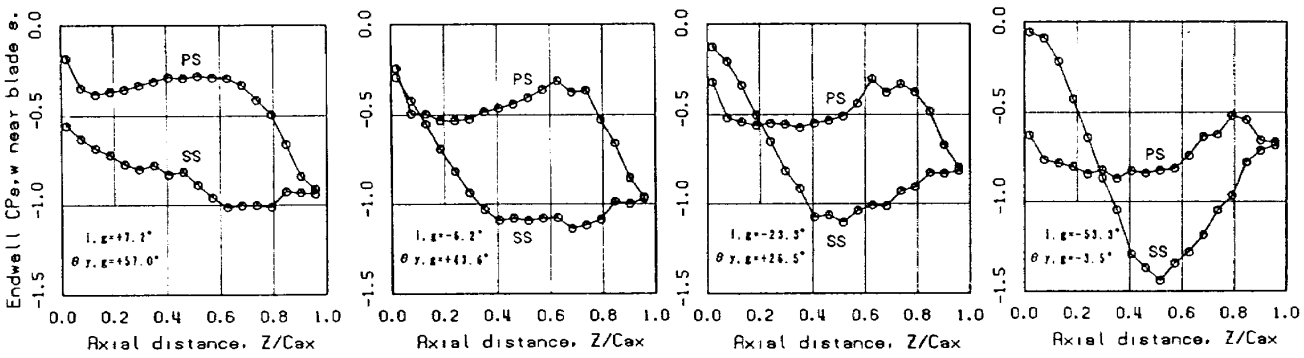

Fig. 16 Tip endwall static pressure around blade surface

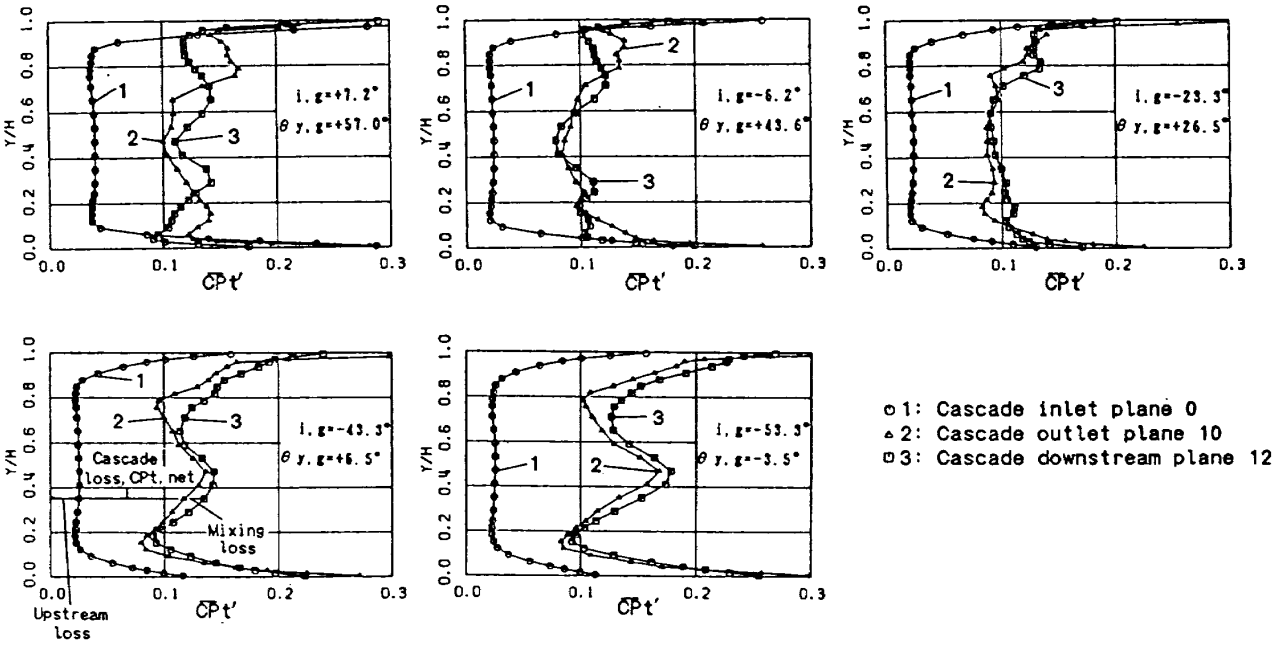

Fig. 17 Evolution of pitch-averaged total pressure loss at three axial locations for five inlet guide angles

(Fig. 9) leads that the effect of incidence on blade loading at the other span would be similar to that shown here. As expected, the loading is affected significantly by the incidence change: The loading in the front part of the cascade passage becomes unloaded as the incidence decreases. Regions with strong adverse pressure gradient (where CP_s increases rapidly with increasing Z/C_{ax}) expand on both blade surfaces; from small regions of the front part of the pressure surface and of the rear part of the suction surface at the maximum incidence, to large regions of the rear part of both blade surfaces at the minimum incidence. The adverse pressure gradient in these regions contributes to the generation of flow separations on both blade surfaces.

Incidence Effects on Overall Loss

Fig. 17 shows spanwise distributions of pitchwise mass-averaged loss obtained at three traverse planes. The loss coefficients CP_t' here were calculated based on the atmospheric pressure and the mass-averaged velocity at the downstream Plane 12. The loss line indicated by 1, therefore, corresponds to the loss due to the natural boundary layer developed on the endwall up to the cascade inlet. The difference between loss lines 1 and 2

corresponds to the net loss generated within the cascade. The net loss, however, does not include all of the wake loss generated by the trailing-edge but does include the majority of the wake loss that can be seen at Plane 10 of Fig. 12 or in Fig. 13. The difference between 2 and 3 corresponds to the mixing loss occurring downstream of the trailing-edge. At the two negative incidences of −43.3 and −53.3 degrees, the mixing loss is generated nearly uniformly along the whole span. The loss peak near the midspan is due to the leading-edge separation. At the two incidences of 7.2 and −6.2 degrees, two loss peaks due to the passage vortices are clearly seen. They move away from the walls as the flow goes downstream from Plane 10 to 12.

Information on the loss evolution throughout cascades is very important as was supplied by several workers (e.g., [3, 4, 7, 11, 12]). In the present study, however, it was difficult to calculate accurately the growth of mass-averaged overall loss in the cascade passage for all traverse planes and incidences tested, due to some difficulties in the mass-average computation of the separated flows. Therefore, only the overall net loss characteristics of the present cascade obtained from the upstream and downstream measurements is shown in Fig. 18. The horizontal axis shows the mass-averaged incidence of the flow at Plane 1. The test loss curve shows very small variation with the incidence, compared to the result predicted by Ainley/Mathieson's method [19]. The method overestimated the overall loss itself for the present cascade, too. For the present, this is presumably because the method tends to overestimate the profile loss $CP_{t,p}$ rather than the secondary loss $CP_{t,s}$, for the present cascade with thick leading- and trailing-edges and high turning.

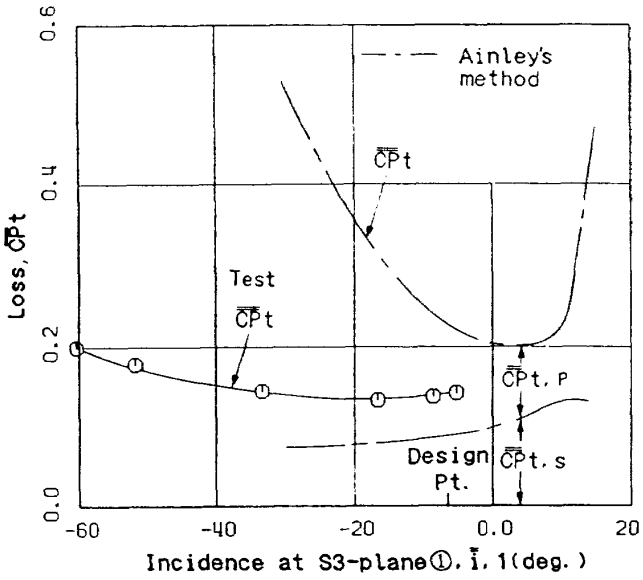

Fig. 18 Overall loss characteristics obtained at S3-plane 12

CONCLUSIONS

The present study revealed many effects of incidence on three-dimensional flows and the loss generation mechanisms in a linear turbine cascade in detail. The results are briefly summarized.

As incidence decreases, the cascade flows near the pressure surface easily separate, and the front part of the cascade becomes unloaded. The separation is the main factor in loss generation especially at smaller (or negative) incidence. The separation generates new secondary flows around the midspan.

The skewness of the endwall flows are very sensitively affected by the incidence variation. As incidence increases, the passage vortices become rapidly intense, which promotes the spanwise flows along the rear part of the blade suction surface. The vortices are the main factors in loss generation at larger (or positive) incidence.

Each vortex occurring within the cascade is sensitive to incidence change. At some negative incidences, the suction-side leg of the leading-edge horseshoe vortex remains up to the cascade exit plane and forms a part of the cascade exit secondary flows. The contribution of the vortex to the cascade loss generation can be recognized only in the endwall loss along the suction surface/endwall corner, but is negligibly small compared to the other losses generated in the cascade such as by the leading-edge flow separation.

Three-dimensional representations of detailed flows and losses presented in the study assist the

cascade extraordinarily complicated flow/loss mechanisms to be understood easily and quantitatively. These give not only a new insight into the cascade flow mechanisms but also solid experimental facts to our knowledge that has already known or speculated.

The overall loss characteristics presently obtained indicate that both the loss variation with incidence change and the loss values themselves are small compared to those predicted by Ainley/ Mathieson Method. Questions remain to be answered if such loss characteristics can hold in other cascades with blunt leading- and trailing-edges and with high turning; tests with other cascades and high-speed real machines, and also further analyses by other methods such as by Dunham and Came [20] are needed.

REFERENCES

1) Ainley, D.G., "The Performance of Axial Flow Turbines," Proc. Instn. Mech. Engrs. 159, p. 235, Fig. 67, 1948.
2) Sjolander, S.A., "The Endwall Boundary Layer in an Annular Cascade of Turbine Nozzle Guide Vanes," Carleton University, TR ME/A 75-4, 1975.
3) Langston, L.S., Nice, M.L., and Hooper, R.M., "Three Dimensional Flow within a Turbine Cascade Passage," ASME Journal of Engineering for Power, Vol. 99, No. 1, pp. 21-28, 1977.
4) Marchal, P., and Sieverding, C.H., "Secondary Flows within Turbomachinery Bladings," Secondary Flows in Turbomachines, AGARD-CP-214, 1977.
5) Carrick, H.B., "Secondary Flow and Losses in Turbine Cascade with Inlet Skew", Secondary Flows in Turbomachines, AGARD-CP-214, 1977.
6) Bindon, J.P., "Exit Plane and Suction Surface Flows in an Annular Turbine Cascade with a Skewed Inlet Boundary Layer," Int. J. Heat and Fluid Flow, Vol. 2, pp. 57-66, 1980.
7) Gregory-Smith, D.G., and Graves, C.P., "Secondary Flows and Losses in a Turbine Cascade," Viscous Effects in Turbomachines, AGARD-CP-351, 1983.
8) Boletis, E., Sieverding, C.H., and Van Hove, W., "Effects of a Skewed Inlet Endwall Boundary Layer on The 3-D Flow Field in an Annular Turbine Cascade," Viscous Effects in Turbomachines, AGARD-CP-351, 1983.
9) Hodson, H.P., and Dominy, R.G., "Three-Dimensional Flow in a Low-Pressure Turbine Cascade at Its Design Condition," ASME Journal of Turbomachinery, Vol. 109, pp. 177-185, 1987.
10) Hodson, H.P., and Dominy, R.G., "The Off-Design Performance of a Low-Pressure Turbine Cascade," ASME Journal of Turbomachinery, Vol. 109, pp. 201-209, 1987.
11) Yamamoto, A., "Production and Development of Secondary Flows and Losses in Two Types of Straight Turbine Cascades, Part 1: A Stator Case," ASME Journal of Turbomachinery, Vol. 108, pp. 186-193, 1987.
12) Yamamoto, A., "Production and Development of Secondary Flows and Losses in Two Types of Straight Turbine Cascades: Part 2: A Rotor Case," ASME Journal of Turbomachinery, Vol. 108, pp. 194-200, 1987.
13) Yamamoto, A., "Interaction Mechanisms between Tip-Leakage Flow and Passage Vortex in a Linear Turbine Rotor Cascade," ASME Journal of Turbomachinery, Vol. 110, pp. 329-338, 1988.
14) Yamamoto, A., "Endwall Flow/Loss Mechanisms in a Linear Turbine Cascade with Blade Tip-Clearance," 88-GT-235, 1988.
15) Langston, L.S., and Boyle, M.T., "A New Surface Streamline Flow Visualization Technique," Journal of Fluid Mechanics, Vol. 125, Dec., pp. 53-57, 1982.

16) Gaugler, R.E., and Russell, L.M., "Comparison of Visualized Turbine Endwall Secondary Flows and Measured Heat Transfer Patterns," ASME Journal of Engineering for Gas Turbine and Power, Vol. 106, pp. 168-172, 1984.

17) Hodson, H.P., "Boundary-Layer Transition and Separation Near the Leading Edge of a High-Speed Turbine Cascade," ASME Journal of Engineering for Gas Turbine and Power, Vol. 107, pp. 127-134, 1985.

18) Bario, F., Leboeuf, F. and Papailliou, K.D., "Study of Secondary Flows in Blade Cascades of Turbomachines," ASME Journal of Engineering for Power, Vol. 104, pp. 497-509, 1982.

19) Ainley, D.G., and Mathieson, G.C.R., "A Method of Performance Estimation for Axial-Flow Turbines," British ARC, RM2974, 1951.

20) Dunham, J., and Came, P.M., "Improvements to Ainley-Mathieson Method of Turbine Performance Prediction," ASME Journal of Engineering for Power, Vol. 92, pp. 252-256, 1970.

TECHNICAL REPORT OF NATIONAL
AEROSPACE LABORATORY
TR-984T

航空宇宙技術研究所報告984T号（欧文）

昭和63年6月発行

発行所 航空宇宙技術研究所
東京都調布市深大寺東町7丁目44番地1
電話三鷹(0422)47-5911(大代表)〒182
印刷所 株式会社 東京プレス
東京都板橋区桜川2－27－12

Published by
NATIONAL AEROSPACE LABORATORY
1,880 Jindaiji, Chōfu, Tokyo
JAPAN

Printed in Japan